

Analysis of Rocket Jet Particulate using Euler-Lagrange and Euler-Euler Approaches

Douglas H. Fontes*, Dana Mikkelsen[†], and Michael P. Kinzel [‡] *University of Central Florida, Orlando, FL, 32816*

Particle laden flows are often modeled using one of two numerical approaches: Euler-Lagrange and Euler-Euler. The Euler-Lagrange approach analyzes the particulate phase from a control mass perspective, then the solid particulate phase is coupled to a (continuous) fluid phase based on the underlying fluid-flow equations formulated within an Eulerian model. The Euler-Euler approach, however, applies the Eulerian formulation for both the fluid and particulate phase. The aim in this effort is to evaluate the approaches in the context of a two-dimensional, compressible gas flow laden with particulate and impinging on a normal surface. Such flows are relevant to classes of solid rockets, sandblast nozzles, and other particleladen flows in the context of converging-diverging nozzles. Several comparisons are made between both approaches. This first pertains to model accuracy of the particulate flow, which involves comparing particle velocities and distributions throughout the numerical domain. In addition, the computational time required to solve particle flow in a compressible gas flow was compared between both numerical approaches. The Euler-Euler approach presented a lower computational time to solve particle flow for the rocket jet compared to the Euler-Lagrange approach. The Euler-Euler approach also showed a lower computational cost than that of the Euler-Lagrange approach to reach a steady solution. Also, a numerical validation of an under-expanded jet case was performed using the Euler-Euler approach. The results of the simulation agreed strongly with experimental measurements.

I. Nomenclature

```
drag force
           lift force
           drag coefficient
C_D
           sum of inertial forces and momentum transfer associated with mass transfer
M
           gravity acceleration [m \cdot s^{-2}]
g
ṁ
           mass transfer rate [kg \cdot s^{-1}]
           total number of phases
Ν
           pressure [Pa]
p
           interfacial heat transfer [W \cdot m^{-3}]
Q
Re
           Reynolds number
T
           temperature [K]
           velocity [m \cdot s^{-1}]
      =
и
           enthalpy [J \cdot kg^{-3}]
h
           particle diameter [m]
d
           strain rate tensor [s^{-1}]
S
k
           kinetic energy [kg \cdot m^2 \cdot s^{-2}]
           position [m]
\boldsymbol{x}
Pr
           pressure ratio
           heat capacity [J \cdot K^{-1}]
c_p
           energy [kg \cdot m^2 \cdot s^{-2}]
e_0
                                           Greek letters
```

^{*}Postdoctoral Researcher, Department of Mechanical and Aerospace Engineering, 4000 Central Florida Blvd.

[†]Undergraduate Research Assistant, Department of Mechanical and Aerospace Engineering, 4000 Central Florida Blvd.

^{*}Assistant Professor, Department of Mechanical and Aerospace Engineering, 4000 Central Florida Blvd.

```
Kronecker delta
δ
            volume fraction
\alpha
            density [kg \cdot m^{-3}]
ρ
            thermal conductivity [W \cdot m^{-1} \cdot K^{-1}]
λ
\sigma_h
            the turbulent thermal diffusion Prandtl number
            shear stress tensor [kg \cdot m^{-1} \cdot s^{-2}]
            molecular viscosity of fluid [kg \cdot m \cdot s^{-1}]
       =
μ
            eddy viscosity (turbulence) model [kg \cdot m \cdot s^{-1}]
\mu_t
                                              Subscript
            axis index
            axis index
k
            axis index
            particle
p
           turbulent
```

II. Introduction

OLID propellant rocket combustors used to propel hypersonic vehicles can involve compressible flow laden with particulate from both the combustion reactants and products. Solid particulates such as aluminum and boron are frequently used in solid propellant rocket combustors to increase the specific impulse of the solid propellant, as it enhances the heat of combustion, propellant density, and combustion temperature [1]. These particulates are accelerated by the gas flow, forming a plume that interacts with the surrounding region. This particulate flow is completely dependent on the gas flow. In reality, the presence of particles also modifies the gas flow. However, for a low volume fraction, the two-way coupling between gas-particle flow can be neglected.

Experimental studies about the gas-particle interactions in rocket jet particulate have been made to evaluate: the effects of compressible flow and normal shocks over the particles inside a nozzle [2]; theoretical description of the behavior of particles, including collision and agglomeration [3]; and damages of the nozzle surfaces [4]. However, due to the limitations of obtaining measurements of gas-particle interaction with no interference and a detailed description of the particle-laden flow, the interactions between gas, particles, and surrounding surfaces, are also addressed via numerical simulation [5–8].

Computational fluid dynamics (CFD) is an one approach to analyze complex multiphase flow, as found in propellant rocket combustors. Compared to experimental approaches, CFD methods are able to provide more information about the characteristics of the gas-particulate flow, with no intrusive interference on it. However, the type of modeling and correlations used in the numerical simulation may not represent suitably the physical phenomena involved in the rocket jet particulate flow.

The numerical simulation of this particulate-laden flow of problem can be performed using different strategies: considering the particulate phase as discrete particles and the gas flow as a continuous phase (Euler-Lagrange); and considering the particulate as a continuous phase alongside the continuous gas flow (Euler-Euler). Numerical simulations using an Euler-Euler approach [9] and an Euler-Lagrange approach [10, 11] have been used to solve solid rocket combustors. In both approaches, the particulate is considered a dispersed phase, whose interaction can be modeled using one-way coupling or two-way coupling. In one-way coupling, the particles are transported by the gas flow, but the gas flow is not affected by the presence of them. On the other hand, in two-way coupling the forces related to the presence of particles in the flow modify the gas flow, according to the Newton's third law. Appropriate models and correlations should be considered in both approaches to suitably address the rocket jet particle flow. Due to the limitations and characteristics of the modelings applied to both Euler-Euler and Euler-Lagrange approaches, slight differences in the numerical solutions are expected between them.

In the present work, numerical simulations of a rocket jet flow with particulate are analyzed considering both Euler-Euler and Euler-Lagrange approaches. The Euler-Euler approach consists of a Dispersed Multiphase Model, as implemented on STAR-CCM+, which can accommodate low volume fraction of particles dispersed in a compressible gas flow. The main goal of this work is to investigate the benefits and deficiencies of each approach for a specific simulation of a particle-laden rocket jet impinging on a normal surface.

III. Methods

A. Numerical Model Formulation

In the present work, a commercial CFD code, STAR-CCM+, version 13.06, [12], is utilized. In general, the numerical solution method couples a gas flow solver to another, modeling the particulate dynamics. The model is developed with assumptions of a steady, axisymmetric, one-way coupling flow. Additional details of the gas solution method and solid-phase model are described below.

1. Eulerian Gas-Phase Numerical Model Formulation

The gas flow solution can be described as a fully coupled, dual-time (not preconditioned), using the Roe flux-difference splitting scheme [13]. The underlying equation set is based on a continuum mass, momentum, and energy conservation equations. To bring this into context, the mass and momentum conservation equations (in a Cartesian basis in index notation) may be described as:

$$\frac{\partial \rho}{\partial t} + \frac{\partial \rho u_i}{\partial x_i} = 0,\tag{1}$$

$$\frac{\partial \left(\rho u_{i}\right)}{\partial t} + \frac{\partial \left(\rho u_{i} u_{j}\right)}{\partial x_{j}} = \frac{\partial \left(-p \delta_{ij} + 2\left(\mu + \mu_{t}\right) S_{ij} - \frac{2}{3} \delta_{ij} \rho k\right)}{\partial x_{j}}.$$
(2)

In the momentum equations, the standard terms are provided along with the molecular viscosity of the fluid, μ , and the eddy viscosity (or turbulence) model, μ_t . The $k - \epsilon$ equations are used to model the turbulence [14].

$$\frac{\partial \rho e_0}{\partial t} + \frac{\partial \left(\rho u_j h\right)}{\partial x_j} = \frac{\partial}{\partial x_j} \left(-\left(\mu + \frac{\mu}{\sigma_k}\right) \frac{\partial k}{\partial x_j} + \left(\frac{c_p \mu}{Pr} + \frac{c_p \mu_t}{Pr_t}\right) \frac{\partial T}{\partial x_j} + 2u_i \left(\mu + \mu_t\right) S_{ij} - \frac{2}{3} \left(\mu + \mu_t\right) u_j \frac{\partial u_k}{\partial x_k} + \frac{2}{3} u_j \rho k \right)$$
(3)

Through these mass, momentum and energy source terms, and the accompany turbulence model, the gas flow dynamics are solved in an Euler reference frame.

2. Euler-Lagrange Multiphase Model

For the Euler-Lagrange approach, only the gas phase is solved as a continuous phase (Eq. 1-3). However, the particulate are modeled as a discrete (particulate) phase, where individual particle trajectories are modeled in a Lagrangian reference frame. Starting from Eq. 4

$$F_i = m_p \ddot{x}_{p,i}. \tag{4}$$

Here, m_p is the particle mass, $\ddot{x}_{p,i}$ is the particle acceleration in the *i* Cartesian direction and F_i is the total force on the particle. F_i can be described as a sum of forces. A primary force here is the drag force $(F_{D,i})$ given as

$$F_{D,i} = \frac{18\mu C_D Re}{24\rho_D d_P^2} \left(\dot{x}_{p,i} - u_i \right), \tag{5}$$

where the Reynolds number, $Re \equiv \frac{\rho d_P |u_i - \dot{x}_{P,i}|}{\mu}$, is calculated considering the relative velocity between particle and gas velocity. The drag coefficient, C_D , is defined using the Schiller and Naumann [15] drag model (which is consistent for both numerical models). The second force considered the weight and buoyant forces on the particle. Other forces, such as the Basset force (added mass) and forces from underlying pressure gradients, are omitted and not anticipated to effect the outcome of the present study.

The numerical solution to the resulting governing equations is modified (Eq. 6) given as:

$$\ddot{x}_{p,i} = F_{D,i} \left(u_i - \dot{x}_{p,i} \right) + \frac{g_i \left(\rho_p - \rho \right)}{\rho_p},\tag{6}$$

Along with the velocity, Eq. 7, so that particle velocity and position can be obtained through temporal integration of the ordinary equations,

$$\dot{x}_{p,i} = u_{p,i},\tag{7}$$

In these equations, $u_{p,i}$ and $x_{p,i}$ are, respectively, the velocity and position vectors of a particle. Additionally, ρ_p is the particle density, ρ is the fluid density, and g_i is the gravity component in the i direction. This solution approach is inherent to STAR-CCM+ and utilized in this work to evaluate its accuracy and computational efficiency.

3. Euler-Euler Multiphase Model

Considering the assumptions made and the Dispersed Multiphase model used in this problem, the representative equations for the Euler-Euler approach consist of the mass conservation, Eq. 8, momentum balance, Eq. 9, and energy conservation, Eq. 11, for each phase, which is represented by the volume fraction, α ,

$$\frac{\partial}{\partial t}\alpha_k \rho_k + \nabla \cdot \alpha_k \rho_k u_k = \sum_{i=1}^N (\dot{m}_{jk} - \dot{m}_{kj}),\tag{8}$$

$$\frac{\partial}{\partial t} \alpha_k \rho_k u_k + \nabla \cdot \alpha_k \rho_k u_k^2 = -\alpha_k \nabla p + \alpha_k \rho_k g + \nabla \cdot \alpha_k (\tau_k + \tau_k^t) + M_k, \tag{9}$$

$$M = F_D + F_L + \sum_{j=1}^{N} (\dot{m}_{jk} u_j - \dot{m}_{kj} u_k), \tag{10}$$

$$\frac{\partial}{\partial t}(\alpha_k \rho_k h_k) + \nabla \cdot (\alpha_k \rho_k u_k h_k) - \nabla \cdot \left[\alpha_k (\lambda_k \nabla T_k + \frac{\mu_t}{\sigma_h} \nabla h_k)\right] = Q_k. \tag{11}$$

IV. Model Validation

Due to the lack of experimental measurements of a real rocket jet particulate flow, a numerical validation of a particle-laden flow [16] was performed using the dispersed multiphase model (Euler-Euler approach) in the present work. The authors of this experimental study evaluated this case using the Euler-Lagrange approach, which showed a good prediction with the measurements.

A. Prior Experimental data for Particle-Laden Compressible Nozzle

An experimental case from Sommerfeld [16] was numerically analyzed using the Euler-Euler approach to solve two-phase flow considering two-way coupling. The experimental case is an under-expanded gas jet with particles, as shown in Fig. 1.

B. Validation Results

A mesh sensitivity study was performed to obtain numerical results independent of the mesh refinement. For the mesh study, a pressure ratio between the inlet and outlet boundaries of $p_r = 33$ was used. The Mach disk standoff distance was obtained and compared for five different mesh resolutions, Tab. 1. Results from these studies are displayed

Table 1 Boundary conditions of the analyzed physical domain.

Mesh	Number of cells	Characteristic length [m]
1	7544	4×10^{-4}
2	10211	3×10^{-4}
3	14714	1.6×10^{-4}
4	31894	8×10^{-5}
5	78191	4×10^{-5}

in Fig. 2. Based on the observed asymptotic result, mesh 4 was used to evaluate different drag coefficient models, pressure ratios, and mass fraction loading.

Comparisons of the Mach disk position, i.e., the distance between the position of the primary normal shock and nozzle exit (Fig. 3(a)), and shape between the experimental and numerical results were performed. In Fig. 3, one can

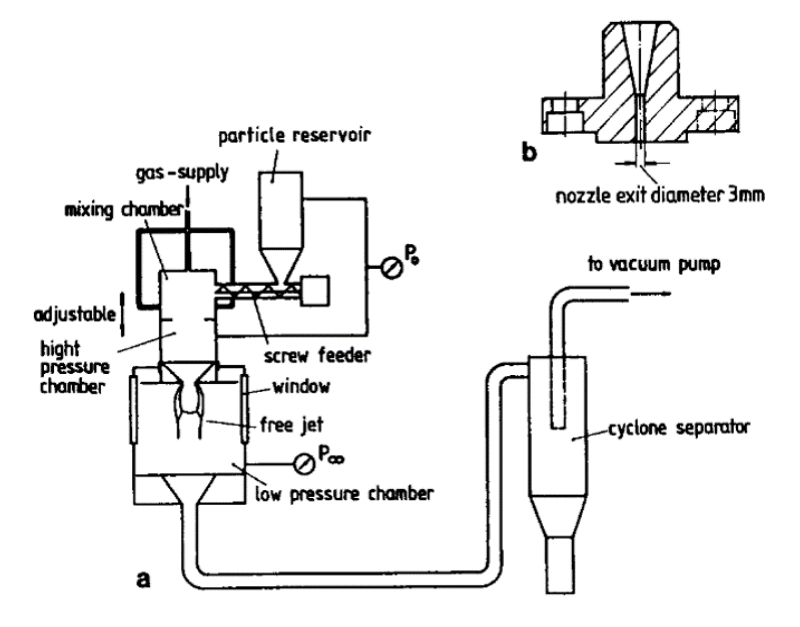


Fig. 1 Diagram of the physical configuration of the underexpanded jet [16].

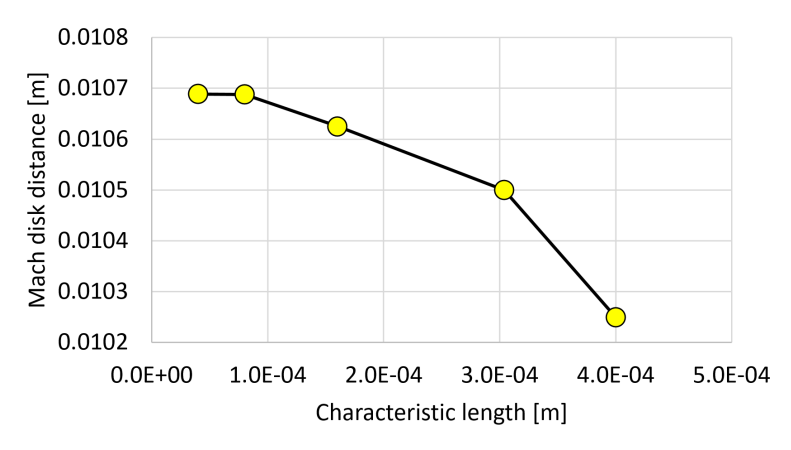


Fig. 2 Mach disk position with mesh refinement.

see some comparisons of the distance of the Mach disk position from the exit nozzle at different pressure ratios as well as a qualitative comparison of the Mach disk shape. The numerical relationship of the Mach disk position with the pressure ratio shows an excellent agreement with the correlation of Ashkenas and Sherman [17], which is based on several experimental measurements. The shape of the Mach disk is well-predicted by the Spalart-Almaras turbulence closure model, as shown in Fig. 3(a). Different turbulence models were tested, such as $k - \epsilon$ and RSM; however, the shape of the Mach disk was not well represented using $k - \epsilon$ and the computational time was significantly increased using RSM.

The effect of mass fraction on the Mach disk position was numerically evaluated according to the experimental conditions studied by Sommerfeld [16]. The interactions between glass particles of $d_p = 45 \mu m$ and the gas flow were simulated using two-way coupling. First and second order schemes were used to solve the particle flow. As shown in Fig. 4, a first-order scheme over-predicts the Mach disk position, while the second-order scheme shows a good agreement with the experimental measurements. As one can see in Fig. 4, the presence of particles in the gas flow pulls the normal shock upstream. The momentum used to accelerate the particles is removed from the gas flow, which reduces the kinetic energy of the gas flow and likewise the Mach disk position.

Despite the fact the discrete particle effects in this case are not solved through the Dispersed Multiphase model (Euler-Euler approach), the continuous solution of particle velocity, particle distribution and the two-way coupling

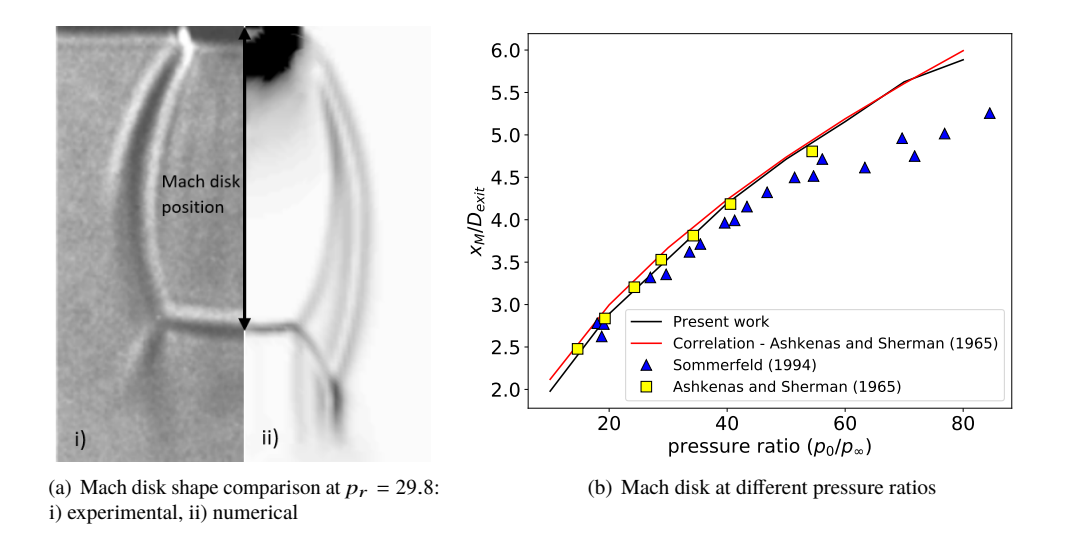


Fig. 3 Comparison of numerical and experimental results of Mach disk position.

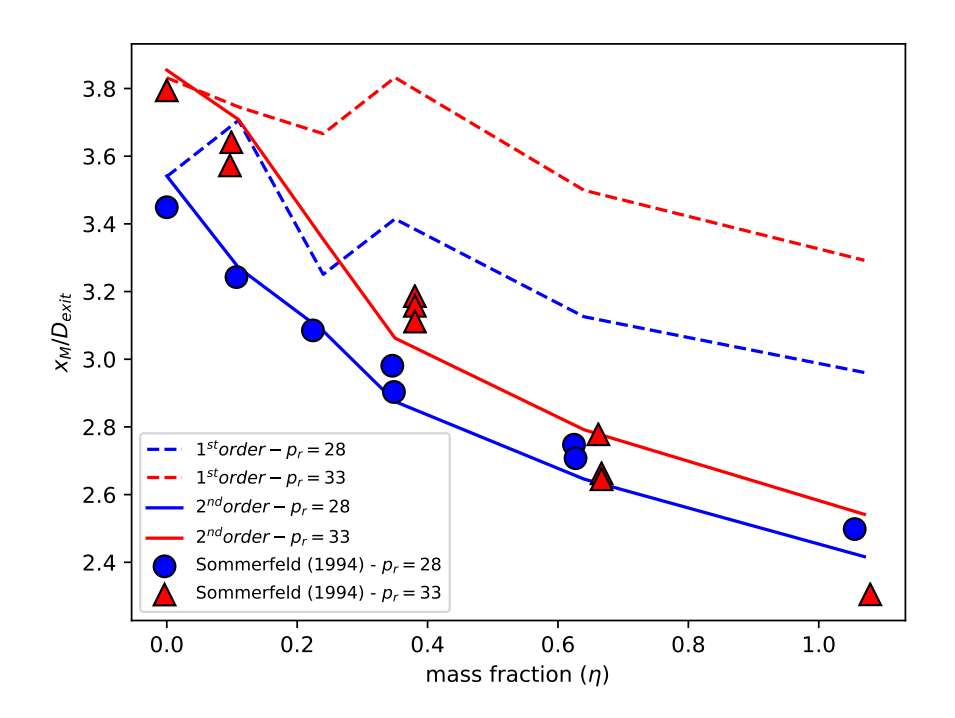


Fig. 4 Mach disk prediction for different mass fractions and pressure ratios.

effects shows a good comparison with experimental data.

V. Results and Discussion

A. Geometry Evaluated

The geometric configuration simulated in the present study is based on an Aerojet Rocketdyne RS-25 rocket nozzle [18]. Where the exact throat dimension was unavailable, an arbitrary dimension was substituted based on the geometric relationships stated in Zhukov [19]. This configuration is represented with a numerical domain detailed in Fig. 5. In the figure the overall dimensions of numerical domain are provided. Here it is important to comment that the domain extends several jet lengths from the nozzle exit. Note that the overall effort, focused on understanding accuracy and time of each method, is not expected to be affected by the boundary location as such biases should equally influence both methods. To reduce computational time, the effort also considers a two-dimensional, axisymmetric domain. In the domain, the nozzle inlet is positioned at 40 m from a normal wall.

B. Boundary Conditions

The boundary conditions of this model, depicted in Fig. 5, are detailed in Table 2. This problem was analyzed

Boundary	Boundary Condition
1	pressure outlet
2	pressure outlet

wall

wall

wall

3

4

5

6

Table 2 Boundary conditions of the analyzed physical domain.

considering both an Euler-Euler approach and an Euler-Lagrange approach. The Euler-Euler approach is based on the Dispersed Multiphase model, which solves the particulate phase as a continuous phase.

stagnation inlet

C. Computational Mesh and Mesh Independence

The axisymmetric domain was discretized using 84094 quadrilateral cells, with higher refinement near wall surfaces and in the gas flow expansion region, as shown in Fig. 6. This mesh, as well as the results in this work, were obtained through the use of STAR-CCM+ software.

In order to isolate the effects of an Euler-Euler model versus an Euler-Lagrange model on the particle flow, an independent mesh was required. Simulations were run with a series of mesh base sizes between $\Delta x = 2.0 \, m$ and $\Delta x = 0.0625 \, m$, with the refinement near the wall surfaces and in the gas flow expansion region dependent upon the base size. The gas velocity along the flow radius at $x = 5 \, m$ (from nozzle exit) was plotted for each mesh, as shown in Fig. 7.

The velocity at the center of the flow $(r/r_t = 0)$ increases significantly from $\Delta x = 2 m$ to $\Delta x = 0.125 m$, but the velocity for $\Delta x = 0.0625 m$ varies little from $\Delta x = 0.125 m$, indicating the mesh has achieved an asymptotic convergence and thus independence. To verify these results, the average gas velocity was calculated over the flow radius at x = 5 m for each mesh, as shown in Fig. 8.

The difference ($\approx 1\%$) in the average gas velocity between $\Delta x = 0.125 \, m$ and $\Delta x = 0.0625 \, m$ indicates the mesh has converged and reached independence. There is little value in further increasing the mesh density, and doing so would result in a more expensive computation. Thus, a base size of $\Delta x = 0.125 \, m$ was chosen for the numerical simulations.

Steady state regime was considered in all simulations. Both approaches utilized a second-order pressure-velocity coupling model and were solved using an unstructured solver. The main parameters for rocket jet simulation with particle injection at the inlet condition were obtained from a numerical simulation of the impact of methane oxidation kinetics on a rocket nozzle flow [19] and experimental data from the analysis of solid-rocket motors [20]. The physical parameters used in the present work are shown in Table 3.

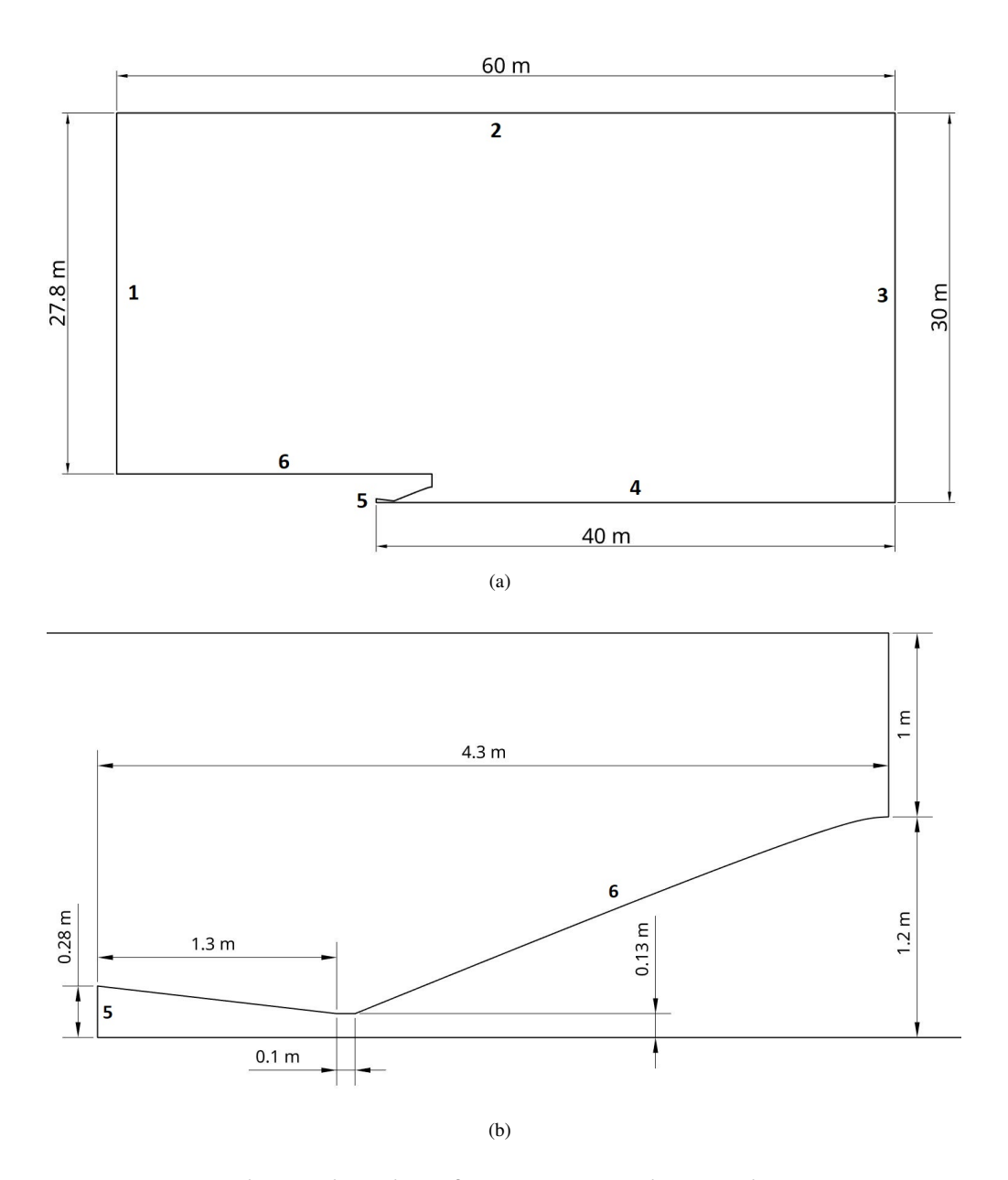


Fig. 5 Dimensions of the analyzed physical domain.

VI. Results Comparing the Approaches

Since the two-phase flow was solved considering one-way coupling for both approaches, the gas flow is the same for both Euler-Euler and Euler-Lagrange approaches. Fig. 9 shows the magnitude of the gas velocity in the domain as well as the magnitude of the particle velocities derived from the Euler-Euler and Euler-Lagrange models.

In terms of the particle velocity, the streamlines of particle velocity are very similar using both approaches. However, the Euler-Lagrange approach predicted a higher value of the maximum particle velocity than the Euler-Euler approach. This difference should be related to the compressible effects inside the nozzle, where the Mach number is higher than 2. The Euler-Euler approach does not account for the compressible effects on the particle transport; it is accounted for in the Euler-Lagrange approach via a pressure term in the transport equations.

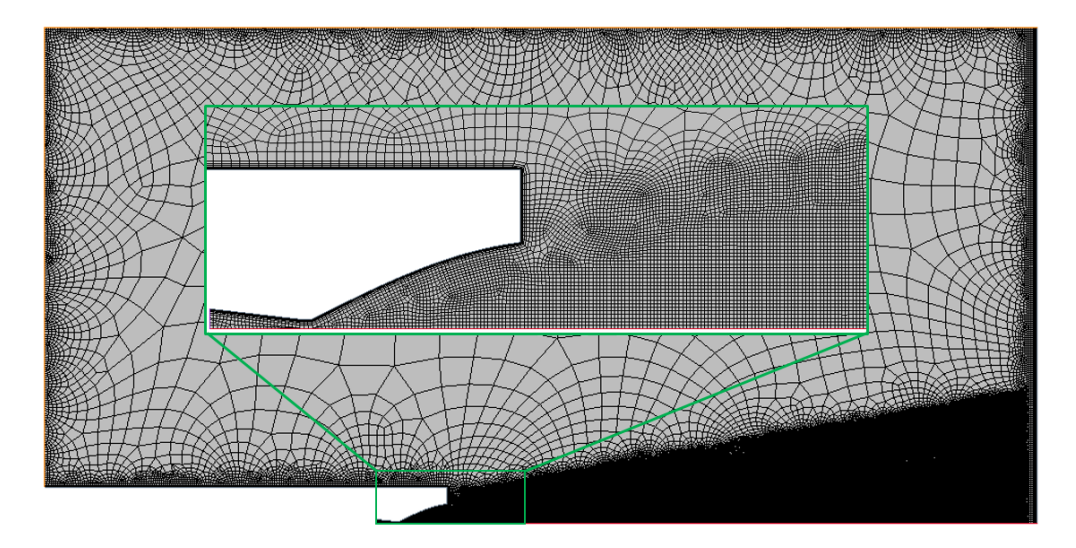


Fig. 6 Numerical mesh of the rocket jet domain.

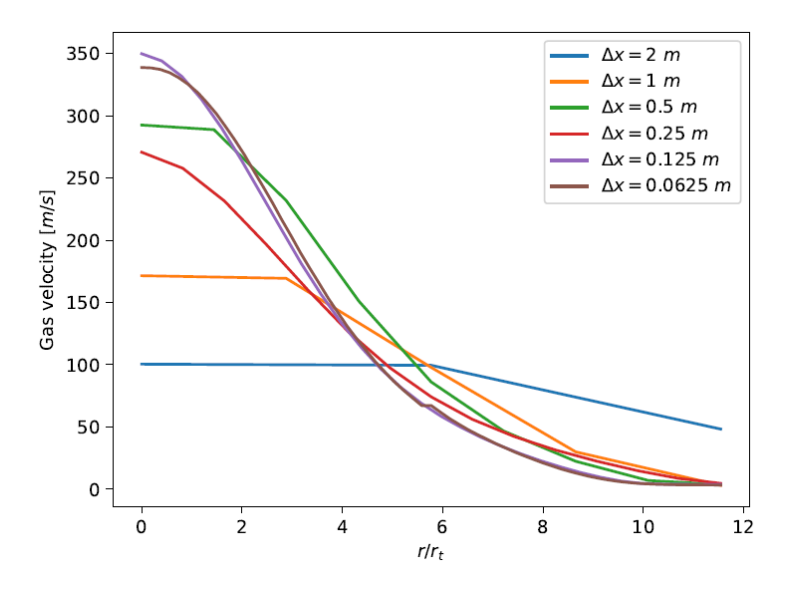


Fig. 7 Gas velocity along radius of flow for increasing mesh density at x = 5 m

A. Particle velocity

Because the properties of the continuous gas phase were identical between simulations due to the one-way coupling model used, only the properties of the particulate phase were analyzed in this study. The first property addressed in this study was the velocity of the particulate. Four line probes were placed from the nozzle exit, respectively, at 5 m, 15 m, 25 m, and 35 m, as shown in Fig. 10. Due to the surrounding quiescent external gas flow, the magnitude of the particle velocity reduces along the longitudinal axis. In addition, the velocity profile becomes flatter with increased distance from the nozzle exit.

The radius of the jet plume increased along the plume as the particles dispersed. Due to the uneven distribution of values obtained from the Euler-Lagrange simulation, the corresponding values for the Euler-Euler simulation were found using linear interpolation. The particle velocity obtained from the Euler-Lagrange simulation was slightly greater than that obtained from the Euler-Euler simulation from x = 5 m to x = 25 m, although the two converged as x increased. The greatest difference between the Euler-Euler and Euler-Lagrange particle velocities occurred at x = 5 m. This difference may be related to the pressure gradient force modeling (only modeled in Euler-Lagrange approach), which is more relevant at regions with higher compressible effects. At x = 35 m, the particle velocities obtained from the two

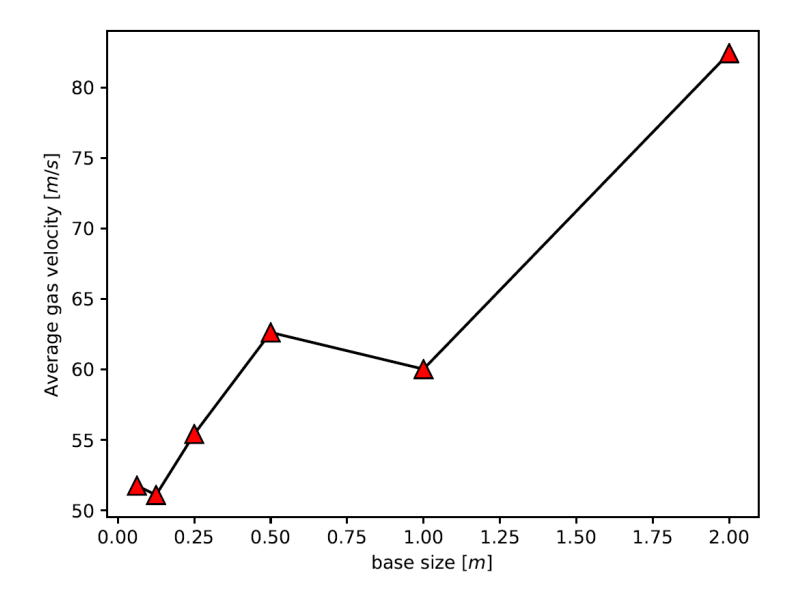


Fig. 8 Average gas velocity for decreasing mesh densities.

Table 3 Main physical parameters for simulation of the rocket jet.

	D	X7.1 .	
	Parameter	Value	
	total inlet pressure	1520 <i>kPa</i>	
	pressure ratio	15	
	exit Mach number	1.39	
	particle diameter	$250 \mu m$	
	particle volume flow rate	$0.1067 m^3/s$	
	particle density	aluminum	
	gas phase	air	
•	Velocity: Magnit 7 0.0000 145.24 290.48 4.	ude (m/s)	
	y 0.0000 145.24 290.48 43	35.72 580.96 726.2.	1
	(a) Magnitude of gas v		1
	ž X		

(b) Magnitude of particle velocity: Euler-Euler Approach (c) Magnitude of particle velocity: Euler-Lagrange Approach

Fig. 9 Gas velocity and particle streamlines in the nozzle region.

simulations were nearly identical, since at this distance compressible effects are less important ($Ma \approx 0.20$). Overall, the particle velocity results obtained from the two approaches were pretty close to each other.

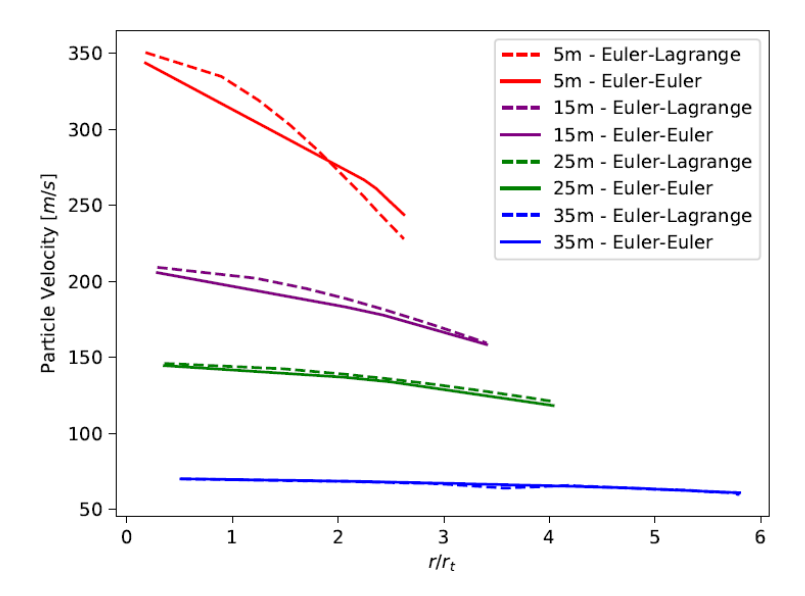


Fig. 10 Particle velocity along the radius of the jet plume.

B. Particle distribution

As indicated above, the radius of the particulate distribution in the flow increased with an increase in *x* along the jet plume. The radii of the particulate distributions are shown in Fig. 11.

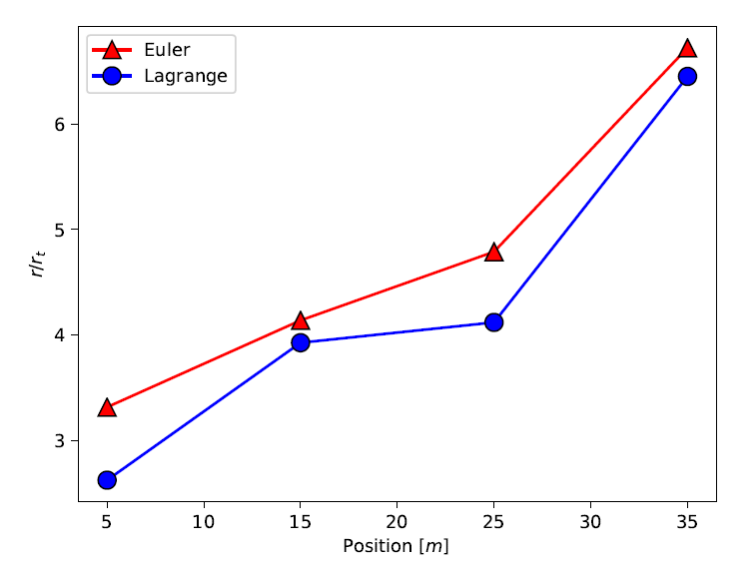


Fig. 11 Radius of particulate distribution vs x-position along jet plume.

The radius of the particulate distribution for the Euler-Euler simulation was measured with the minimum volume fraction set at $\alpha = 5e - 4$. For the Euler-Lagrange simulation, the streamlines provided by the track file acted as the boundary. The results obtained for the Euler-Euler simulation were dependent on the selected minimum volume fraction. The streamlines of the Euler-Lagrange simulation stood independently.

The radius of the particle distribution obtained from the Euler-Euler simulation increased linearly from x = 5 m to x = 25 m. The particle distribution in the Euler-Lagrange simulation was not linear between x = 5 m and x = 25 m. The sharp increase between x = 25 m and x = 35 m in both simulations was due to the flow hitting the impinging wall at x = 40 m.

C. Computational time

It has been previously indicated that Euler-Lagrange numerical modeling approaches are more computationally expensive than Euler-Euler simulations [21, 22]. The results of this study followed these predictions, as shown in Fig 12.

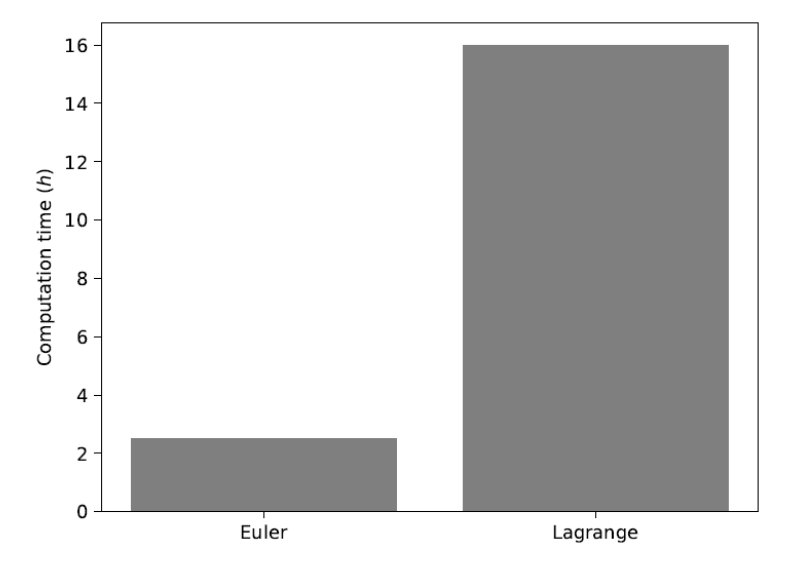


Fig. 12 Computation time of particulate phase.

Due to computational load, each simulation was run using one-way coupling between the gaseous phase and the particulate phase; therefore, these results indicate the computation time for the particulate phase alone. The Euler-Euler simulation completed in 2.49 h - 6.4 times faster than the Euler-Lagrange simulation, which completed in 15.97 h.

VII. Conclusion

In the present work, numerical analysis of rocket jet particulate flow using two approaches were performed numerically. A validation case of an under-expanded gas jet laden with particles was simulated using an Euler-Euler approach. The numerical predictions of normal shock position as shape agreed well with experimental data. Two-way coupling with a second-order discretization scheme was able to predict the gas flow velocity and the position of normal shock satisfactorily.

Regarding the rocket jet particulate simulations, both approaches (Euler-Lagrange and Dispersed Multiphase (Euler-Euler) approaches) are able to properly solve particle velocity and distribution in a compressible flow with high gas velocities. The models used for this problem utilized one-way coupling between the gaseous and particulate phases; therefore, only differences in particulate behavior were observed. The Euler-Euler simulation was 6.4 times faster than the Euler-Lagrange to simulate the same case, and the resultant particle velocities from each simulation agreed very well with each other. The radial distribution of particles shows slightly differences between the two approaches. Those differences are more pronounced close to the nozzle exit, which may be due to the strong compressible effects. The Euler-Lagrange approach models the compressible effects through the pressure gradient term, while the Euler-Euler approach does not have implemented on STAR-CCM+ the pressure gradient term.

Taking into account run-time and accuracy, the present study indicates the Euler-Euler approach using the Dispersed Multiphase model is a suitable numerical model to analyze the flow of rocket-jet particulate. However, further analysis should be made on the modeling of this kind of two-phase flow, such as evaluation of two-way coupling on the gas and particle flow, pressure gradient term, effects of volume fraction, and different particle diameters. In addition, for a better understanding of the capabilities of the numerical modelings, the numerical results should be compared to future experimental measurements related to the rocket-jet particulate flow regime.

References

[1] Chaturvedi, S., and Dave, P. N., "Solid propellants: AP/HTPB composite propellants," Arabian Journal of Chemistry, 2015.

- [2] Soo, S. L., "Gas dynamic processes involving suspended solids," *AIChE Journal*, Vol. 7, No. 3, 1961, pp. 384–391. doi:10.1002/aic.690070308, URL https://aiche.onlinelibrary.wiley.com/doi/abs/10.1002/aic.690070308.
- [3] Sternin, L. E., "Fundamentals of gasdynamics of two-phase nozzle flows," Moscow Izdatel Mashinostroenie, 1974.
- [4] Klager, K., "The Interaction of the Efflux of Solid Propellants with Nozzle Materials," Propellants, Explosives, Pyrotechnics, Vol. 2, No. 3, 1977, pp. 55-63. doi:10.1002/prep.19770020304, URL https://onlinelibrary.wiley.com/doi/abs/10.1002/prep.19770020304.
- [5] Ciucci, A., Iaccarino, G., Ciucci, A., and Iaccarino, G., "Numerical analysis of the turbulent flow and alumina particle trajectories in solid rocket motors," 33rd Joint Propulsion Conference and Exhibit, 1997. doi:10.2514/6.1997-2860, URL https://arc.aiaa.org/doi/abs/10.2514/6.1997-2860.
- [6] Troyes, J., Dubois, I., Borie, V., and Boischot, A., "Multi-Phase Reactive Numerical Simulations of a Model Solid Rocket Exhaust Jet," 42nd AIAA/ASME/SAE/ASEE Joint Propulsion Conference & Exhibit, 2006. doi:10.2514/6.2006-4414, URL https://arc.aiaa.org/doi/abs/10.2514/6.2006-4414.
- [7] Songjiang, F., Wansheng, N., Qingfen, X., and Liwei, D., "Numerical Simulation of flow field and radiation of an aluminized solid-propellant rocket multiphase exhaust plume," *39th AIAA Thermophysics Conference*, 2007. doi:10.2514/6.2007-4415, URL https://arc.aiaa.org/doi/abs/10.2514/6.2007-4415.
- [8] Maochang, D., Xijun, Y., Dawei, C., Fang, Q., and Shijun, Z., "Numerical Simulation of Gas-Particle Two-Phase Flow in a Nozzle with DG Method," *Discrete Dynamics in Nature and Society*, Vol. 2019, 2019, pp. 1–12. doi:10.1155/2019/7060481.
- [9] Binauld, Q., Lamet, J.-M., Tessé, L., Rivière, P., and Soufiani, A., "Numerical simulation of radiation in high altitude solid propellant rocket plumes," *Acta Astronautica*, Vol. 158, 2019, pp. 351 360. doi:https://doi.org/10.1016/j.actaastro.2018.05.041, URL http://www.sciencedirect.com/science/article/pii/S0094576518303606.
- [10] Li, Y., Ren, D., Bo, Z., Huang, W., Ye, Q., and Cui, Y., "Gas-particle two-way coupled method for simulating the interaction between a rocket plume and lunar dust," *Acta Astronautica*, Vol. 157, 2019, pp. 123 133. doi:https://doi.org/10.1016/j.actaastro.2018.12.024, URL http://www.sciencedirect.com/science/article/pii/S0094576518315637.
- [11] Li, Z., Wang, N., Shi, B., Li, S., and Yang, R., "Effects of particle size on two-phase flow loss in aluminized solid rocket motors," *Acta Astronautica*, Vol. 159, 2019, pp. 33 40. doi:https://doi.org/10.1016/j.actaastro.2019.03.022, URL http://www.sciencedirect.com/science/article/pii/S0094576518320769.
- [12] Cd-Adapco, STAR-CCM+ documentation, Siemens, 2018.
- [13] Roe, P. L., "Characteristic-Based Schemes for the Euler Equations," *Annual Review of Fluid Mechanics*, Vol. 18, No. 1, 1986, pp. 337–365. doi:10.1146/annurev.fl.18.010186.002005, URL https://doi.org/10.1146/annurev.fl.18.010186.002005.
- [14] Ferziger, J. H., and Perić, M., Computational Methods for Fluid Dynamics, third edition ed., Springer Berlin Heidelberg, Germany, 2002.
- [15] Schiller, L., and Naumann, A., "A drag coefficient correlation," Zeitschrift des Vereins Deutscher Ingenieure, Vol. 77, 1935, pp. 318–320.
- [16] Sommerfeld, M., "The structure of particle-laden, underexpanded free jets," Shock Waves, Vol. 3, No. 4, 1994, pp. 299–311. doi:10.1007/BF01415828.
- [17] Ashkenas, H., and Sherman, F. S., "Structure and Utilization of Supersonic Free Jets in Low Density Wind Tunnels," Tech. rep., Jet Propulsion Laboratory, 1965.
- [18] Galvez, R., Gaylor, S., Young, C., Patrick, N., Johnson, D., and Ruiz, J., "The Space Shuttle and Its Operations,", Aug. 2011. URL https://www.nasa.gov/centers/johnson/pdf/584722main_Wings-ch3a-pgs53-73.pdf.
- [19] Zhukov, V. P., "The impact of methane oxidation kinetics on a rocket nozzle flow," Acta Astronautica, Vol. 161, 2019, pp. 524 530. doi:https://doi.org/10.1016/j.actaastro.2019.01.001, URL http://www.sciencedirect.com/science/article/pii/S0094576518315066.
- [20] Hovland, D. L., "Particle sizing in solid rocket motors,", 1989. URL https://calhoun.nps.edu/handle/10945/26153.
- [21] Murrone, A., and Villedieu, P., "Numerical Modeling of Dispersed Two-Phase Flows," *AerospaceLab*, 2011, pp. p. 1–13. URL https://hal.archives-ouvertes.fr/hal-01181241.
- [22] Toschi, F., and Bodenschatz, E., "Lagrangian Properties of Particles in Turbulence," Annual Review of Fluid Mechanics, Vol. 41, No. 1, 2009, pp. 375–404. doi:10.1146/annurev.fluid.010908.165210, URL https://doi.org/10.1146/annurev.fluid.010908.165210.